

# Structure and composition of the subcontinental lithospheric mantle beneath the Sangilen Plateau (Tuva, southern Siberia, Russia): Evidence from lamprophyre-hosted spinel peridotite xenoliths

Zoltán Konc<sup>a,\*</sup>, Claudio Marchesi<sup>a</sup>, Károly Hidas<sup>a</sup>, Carlos J. Garrido<sup>a</sup>, Csaba Szabó<sup>b</sup>, Victor V. Sharygin<sup>c</sup>

<sup>a</sup> Instituto Andaluz de Ciencias de la Tierra (IACT), CSIC-UGR, Armilla, Granada, Spain

<sup>b</sup> Lithosphere Fluid Research Lab, Eötvös University, Budapest, Hungary

<sup>c</sup> V.S. Sobolev Institute of Geology and Mineralogy SD RAS, Novosibirsk, Russia

## ARTICLE INFO

### Article history:

Received 22 February 2012

Accepted 15 May 2012

Available online 23 May 2012

### Keywords:

Subcontinental mantle xenoliths

Spinel peridotite

Partial melting

Mantle metasomatism

Sangilen Plateau

Siberia

## ABSTRACT

We present new data on spinel peridotite xenoliths hosted in Agardag alkaline lamprophyres from the Sangilen Plateau (Tuva, South Siberia, Russia), sampling at ~450 Ma the subcontinental lithospheric mantle of the Tuva-Mongolian micro-continent that belongs to the accretionary Central Asian orogenic belt at the southern edge of the Siberian craton. Xenoliths are spinel lherzolites principally showing poikilitic and subordinately coarse granular and coarse equigranular textures. Geothermobarometric calculations for pyroxene yield a narrow range of equilibration temperature (ca. 1000–1100 °C) that corresponds to lithospheric depths from 43 to 53 km (1.3–1.6 GPa) along a hot intracontinental geotherm. Variation of mean Mg# [100\*Mg/(Mg + Fe)] of olivine (87.9–90.9) with mean Cr# [100\*Cr/(Cr + Al)] of spinel (9.5–45.7) indicates that spinel lherzolites are mostly residues of up to 10% melting of a fertile peridotite source. In terms of normalized REE (Rare Earth Element) and incompatible trace element patterns of clinopyroxene, the Sangilen xenoliths can be classified into three types: Type I characterized by convex-upward REE patterns depleted in LREE ( $0.10 \leq \text{La/Yb}_N \leq 0.49$ ), and with relative negative anomalies of Rb, Pb, Hf, Zr and Ti and positive spikes of U and Sr; Type II displaying variable LREE/HREE ratios ( $0.53 < \text{La/Yb}_N < 2.17$ ) but generally flatter REE patterns) and similar abundances of other trace elements compared to Type I; and Type III showing a LREE enriched pattern [(La/Sm)<sub>N</sub> = 2.22; (La/Yb)<sub>N</sub> = 8.42], high REE contents and no relative anomalies of U and Sr. The elevated Yb<sub>N</sub> concentration of one Type II clinopyroxene and the variable fractionation of LREE-MREE relative to HREE in most xenolith types indicate Sangilen xenoliths underwent variable metasomatic enrichment. This enrichment is well accounted by percolation-reaction between depleted peridotite and small-melt fractions of alkaline mafic melts precursor to the Agardag alkaline lamprophyres. The lack of correlation with depth of modal variations, textural types, inferred degrees of melting and trace element patterns in xenoliths indicates the absence of a texturally or compositionally layered lithospheric mantle sampled by Ordovician lamprophyres beneath the Sangilen plateau. The observed compositional variations are better accounted by depleted lithosphere variably metasomatized along a network of percolating alkaline mafic melts heterogeneously distributed throughout the Sangilen lithospheric mantle section.

© 2012 Elsevier B.V. All rights reserved.

## 1. Introduction

Our knowledge of the composition and magmatic record of the subcontinental upper mantle comes from the investigation of peridotite from a variety of tectonic settings including mantle sections tectonically obducted as orogenic peridotite massifs, peridotite xenoliths – primarily spinel peridotite – erupted in tectono-magmatically active areas away from cratons, and peridotite xenoliths – spinel and garnet peridotite –

carried by kimberlites erupted through both Archean and middle to early Proterozoic crust (Bodinier and Godard, 2006; Carlson et al., 2005; Downes, 2001; Pearson et al., 2003; and references therein). In particular, the trace element geochemistry and microstructure of mantle xenoliths hosted in Paleozoic lamprophyre and lamproite at the southern edge of the Siberian craton are poorly known, and their study hence provides a unique opportunity to investigate the nature of the subcontinental mantle beneath these terrains. In this paper we present new data on spinel xenoliths hosted in Early Ordovician alkaline lamprophyres from the Sangilen Plateau (Tuva, Russia) in the accretionary Central Asian orogenic belt, (southern Siberia) (Fig. 1). These lamprophyre-hosted spinel peridotite xenoliths allow us to investigate

\* Corresponding author. Tel.: +34 958230000; fax: +34 958552620.  
E-mail address: [zoltankonc@iact.ugr-csic.es](mailto:zoltankonc@iact.ugr-csic.es) (Z. Konc).

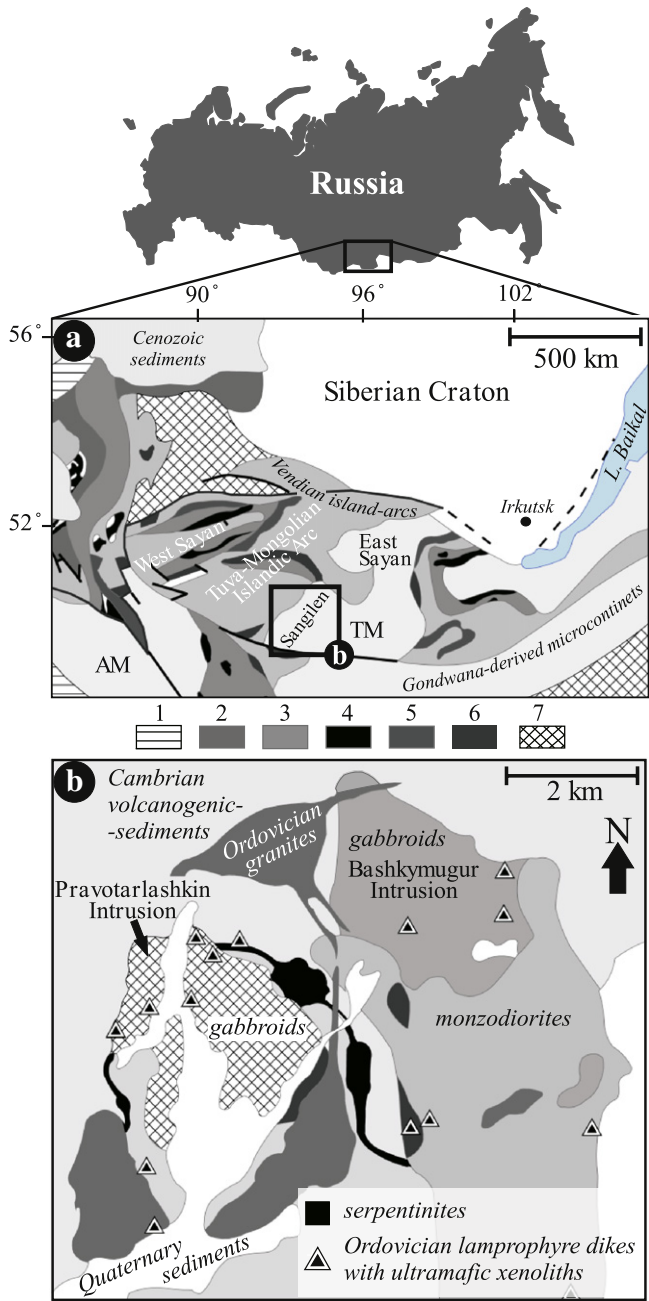


**Fig. 1.** (a) Simplified geological map of the Central Asian Orogenic Belt in southern Russia (inset) (modified after Dobretsov and Buslov, 2007). AM and TM refers respectively to the Gondwana derived micro-continents of Altai-Mongolian and Tuva-Mongolian. Legend of tectonic units: 1: Hercynides; 2: Cambrian island arc calc-alkaline volcanic series; 3: Neoproterozoic-Cambrian accretionary prisms; 4: Neoproterozoic-Cambrian ophiolites; 5: Neoproterozoic supra-subduction ophiolites; 6: Neoproterozoic-Cambrian ophiolitic basalts; 7: Middle-Late Paleozoic volcano-sedimentary basins; (b) Simplified geological map of the Sangilen Plateau (see inset in Fig. 1a) showing the location of the intrusive Ordovician Agardag lamprophyre dikes containing mantle peridotite xenoliths (modified after Egorova et al., 2006).

the composition and thermal structure of the circumcratonic subcontinental lithospheric mantle of the Tuva-Mongolian micro-continent (Griffin et al., 1999b), (Fig. 1a). Sangilen mantle xenoliths therefore offer complementary information on the Central Asia subcontinental mantle lithosphere to that provided by mantle xenoliths in younger Neogene basalts that sample the subcontinental mantle beneath the Baikal rift and Mongolia (e.g., Ionov, 2002; Litasov et al., 2000; Wiechert et al., 1997).

## 2. Geological setting

The Central Asian orogenic belt was formed by accretion of continental, oceanic and island arc tectonic blocks at the southern edge of the Siberian craton during the Neoproterozoic and Paleozoic (Berzin et al., 1994; Mossakovskii et al., 1993). One of the largest blocks accreted during this orogeny was the Tuva-Mongolian micro-continent, whose southwestern part is constituted by the Sangilen Plateau (Fig. 1a) (Vladimirov et al., 2005). This plateau is primarily made up of amalgamated metamorphic and igneous complexes (Fig. 1b) that were first interpreted as the Archean-Paleoproterozoic basement of the Tuva-Mongolian micro-continent (Ilyin, 1990; Zonenshain et al., 1990). However, later studies have shown that these rocks are not related to the Proterozoic accretion, but they are Cambrian-Ordovician metamorphic and plutonic complexes (Izokh et al., 2001). These complexes are intruded by ultramafic to felsic igneous rocks (Izokh et al., 2001; Vladimirov et al., 2005) (Fig. 1b). One of the youngest igneous episodes (447–441 Myr) formed the Agardag alkaline lamprophyre dike complex (Gibsher et al., 2012; Izokh et al., 2001; Vladimirov et al., 2005) (Fig. 1b; dark triangles). Agardag alkaline lamprophyres are camptonites (Izokh et al., 2001); in terms of total alkalis ( $\text{Na}_2\text{O} + \text{K}_2\text{O}$ ) versus  $\text{SiO}_2$  content they are characterized by high alkalis and low  $\text{SiO}_2$  contents similar to foidite and basanite lavas (Rock, 1991). These lamprophyre dikes are intrusive into the Moren metamorphic complex, the Cambrian volcanogenic-sedimentary units, the Pravotarlashkin troctolite-anorthosite-gabbro complex, and the Ordovician Bashkymugur gabbro-norite and monzodiorite (Fig. 1b) (Izokh et al., 2001; Vladimirov et al., 2005). These lamprophyre dikes contain rare mantle xenoliths (Egorova et al., 2006) that are the subject of the present study and will be referred to as Sangilen xenoliths.

## 3. Sampling and petrography

The studied Sangilen xenoliths were sampled from different localities of the Agardag alkaline lamprophyre dike complex (Fig. 1b) and are invariably spinel lherzolites. Peridotite xenoliths in these dikes can be up to 10 cm in diameter, they are commonly highly altered and friable. Fresh peridotite xenoliths are uncommon and small, limiting the availability of samples for the present study and preventing their bulk rock analysis. For this study, we selected highly fresh peridotite xenoliths (up to 4 cm in size) representative of the textural and modal variations of the suite (Table 1). The modal composition of xenoliths was estimated by image analyses of thin sections (Table 1). The selected xenoliths lack any vein or modal layering and are spinel lherzolites with variable modal proportions of olivine, orthopyroxene and clinopyroxene (Table 1). Sangilen xenoliths show principally poikilitic texture (e.g., Downes et al., 1992; Gregoire et al., 1997; Mercier and Nicolas, 1975; Xu et al., 1998) characterized by coarse (3–4 mm) orthopyroxene enclosing olivine (1–2 mm) (Fig. 2a); less common coarse equigranular texture has homogeneous (0.5–2 mm) grain size (Fig. 2b), and coarse granular texture (Lenoir et al., 2000; Mercier and Nicolas, 1975) has relatively large olivine (up to 3 mm) and pyroxenes (1–2 mm) (Fig. 2c). Coarse equigranular and coarse granular xenoliths not only differ in terms of olivine grain size but also in the shape of grain boundaries, which is, respectively, straight (Fig. 2b) and curvilinear (Fig. 2c). Pyroxenes show no exsolution lamellae and round sub-hedral spinel grains occur either interstitially (sometimes with holy-leaf shape) or as inclusions in silicates (Fig. 2b, c). Spinel grains are always smaller (0.5–1 mm) than other rock-forming minerals. Sulfide blebs (30–300  $\mu\text{m}$ ) are common in all samples.

## 4. Instrumental analysis

Electron probe microanalyses were carried out using a JEOL Superprobe JXA 8100 and a CAMECA SX50 instruments at the Institute

of Geology, Siberian Branch of the Russian Academy of Science in Novosibirsk (Russia). Accelerating voltage was 20 kV, sample current 7 nA and beam diameter 5  $\mu\text{m}$ . Counting time for each element was 10 s. Natural and synthetic silicate and oxide standards were used for calibration and ZAF correction. The average major element contents of minerals in the studied samples are reported in Table 1.

In situ analyses of trace elements in clinopyroxene were carried out by Laser Ablation Inductively Coupled Plasma Mass Spectrometry (LA-ICP-MS). Analyses were performed at Géosciences Montpellier (CNRS-University of Montpellier II, Montpellier, France) using a ThermoFinnigan ELEMENT XR sector field ICP-MS, coupled with a Geolass (Microlas) automated platform housing a 193 nm Complex 102 laser from LambdaPhysik. Ablation was conducted in a cell of ca. 30  $\text{cm}^3$  in He atmosphere, which enhances sensitivity and reduces inter-element fractionation. Signals were acquired devoting 2 min for the background blank and 1 min for measurement of the sample. The laser was fired at an energy fluency of 15  $\text{J}/\text{cm}^2$  and a frequency of 6 and 8 Hz using circular spot sizes of 102 and 122  $\mu\text{m}$  in diameter, respectively. Concentrations were calibrated against the NIST Certified Reference rhyolite glass 612, using the values compiled by Pearce et al. (1997). Data were subsequently reduced using the GLITTER software (Van Achtebergh et al., 2001) by inspecting the time-resolved analyses to check for lack of heterogeneities in the analyzed volume. CaO was used as internal standard and BIR-1 G (USGS basaltic glass reference sample) was shot in every procedure for analytical quality control. Average trace element analyses of clinopyroxene are given in Table 2.

## 5. Mineral chemistry

### 5.1. Major elements

In terms of major elements, olivine, orthopyroxene, clinopyroxene and spinel are homogenous at the thin section scale. Average Mg# [ $100 \cdot \text{Mg}/(\text{Mg} + \text{Fe})$ ] of olivine is uncorrelated with the textural type of xenoliths and ranges from 87.9 to 90.9 as characteristic for fertile lherzolite (Fig. 3). Average Mg# of orthopyroxene ranges from 88.4 to 91.5, CaO from 0.85 to 1.08 wt.%, and  $\text{Al}_2\text{O}_3$  from 4.18 to 5.70 wt.% except in lherzolites 3H-2 and 5H-13 where the  $\text{Al}_2\text{O}_3$  content is significantly lower (2.79–2.88 wt.%) (Table 1). Clinopyroxene (Mg-augite) has an average Mg# ranging from 88.2 to 91.8 and highly variable  $\text{Al}_2\text{O}_3$  content (3.49–7.64 wt.%).  $\text{Cr}_2\text{O}_3$  and  $\text{Na}_2\text{O}$  contents span from 0.73 to 1.64 wt.% and 0.87 to 1.75 wt.%, respectively (Table 1). Average Cr# [ $100 \cdot \text{Cr}/(\text{Cr} + \text{Al})$ ] of spinel (Mg–Al chromite) is highly variable (9.5–45.7) (Fig. 3) and Mg# ranges between 63.9 and 78.2. These compositions are similar to those reported in previous studies of major elements in minerals from the Sangilen xenoliths (Egorova et al., 2006; Gibsher et al., 2008) and are typical of mantle-derived spinel lherzolite xenoliths (e.g., Maaloe and Aoki, 1977; Pearson et al., 2003).

### 5.2. Trace elements in clinopyroxene

Clinopyroxene has homogenous trace element composition in each sample. Three types of chondrite-normalized (Sun and McDonough, 1989) rare earth element (REE) patterns of clinopyroxene can be differentiated:

- (i) Type I: characterized by convex-upward patterns depleted in light REE (LREE) with  $0.12 \leq \text{La}/\text{Sm}_N \leq 0.45$  and  $0.10 \leq \text{La}/\text{Yb}_N \leq 0.49$  in samples 3H-4, 3H-8, 5H-7 and 5H-9 (Fig. 4a);
- (ii) Type II: characterized by relatively flat REE patterns with  $0.65 \leq \text{La}/\text{Sm}_N \leq 1.59$  and  $0.53 \leq \text{La}/\text{Yb}_N \leq 2.17$  in samples 3H-2, 5H-2, 5H-3 and 5H-10 (Fig. 4b);
- (iii) Type III: characterized by enriched LREE patterns with average  $(\text{La}/\text{Sm})_N = 2.22$  and  $(\text{La}/\text{Yb})_N = 8.42$  in xenolith 5H-13 (Fig. 4c).

The shape of normalized patterns of clinopyroxene is unrelated to its modal abundances and/or textural type of xenoliths.

Primitive upper mantle (PUM) normalized (Sun and McDonough, 1989) multi-element patterns of clinopyroxene in Sangilen xenoliths also vary according to the groups differentiated on the basis of REE: (i) Type I xenoliths have trace element abundances that generally increase towards the least incompatible elements from  $\sim 0.01$  to  $10 \times \text{PUM}$ . Exceptions to this trend are relative negative anomalies of Rb, Pb, Hf, Zr and Ti and positive spikes of U and Sr (Fig. 4d); (ii) Type II xenoliths display concentrations and spikes similar to Type I in the PUM normalized multi-element diagrams but less patent positive anomalies of U (Fig. 4e); the trace element abundances of clinopyroxene in 5H-10 are remarkably higher than in other samples, mostly  $> 10 \times \text{PUM}$ ; finally, (iii) Type III xenolith 5H-13 generally displays trace element concentrations between 1 and  $10 \times \text{PUM}$  with no relative anomalies of U and Sr, and a negative Nb spike (Fig. 4f).

## 6. Discussion

### 6.1. Depth of provenance of xenoliths and thermal structure of the lithospheric mantle beneath the Sangilen Plateau

The spinel lherzolite assemblage of the Sangilen xenoliths indicates they are samples coming from lithospheric depths above the spinel to garnet lherzolite facies transition (Fig. 5) Due to the lack of accurate geobarometric formulations for spinel lherzolite (Nimis and Grütter, 2010; Taylor, 1998; and references therein), the depth of provenance of the Sangilen xenoliths can only be assessed combining the calculated equilibration temperature of mantle xenoliths with the inferred mantle paleogeotherm at the age of intrusion of the Agardag lamprophyres. Calculated equilibration temperatures of Sangilen xenoliths, obtained using several recommended geothermometric formulations for spinel peridotite, are reported in Table 1 ( $T_{\text{Cpx-Opx}}$ , two-pyroxene geothermometer of Taylor, 1998;  $T_{\text{Ca-Opx}}$ , Ca-in-orthopyroxene geothermometer of Brey and Köhler, 1990;  $T_{\text{Ca-Opx-mod}}$ ,  $T_{\text{Ca-Opx}}$  formulation modified by Nimis and Grütter, 2010; and  $T_{\text{Cr-Al-Opx}}$ , the Al-in-orthopyroxene geothermometer of Witt-Eickchen and Seck, 1991). Most geothermometric formulations yield a relatively narrow range of equilibration temperature ( $\sim 1000$ – $1100$  °C) (Table 1). An exception is sample 5H-10 for which the  $T_{\text{Cpx-Opx}}$  geothermometer yields an unusually low equilibration temperature ( $\sim 850$  °C) relative to that obtained from other thermometric formulations (Table 1). This divergence is common in spinel mantle xenoliths and reflects lack of chemical disequilibrium between orthopyroxene and clinopyroxene (Nimis and Grütter, 2010). The lack of textural evidence for secondary clinopyroxene and the high temperature obtained for the  $T_{\text{Cr-Al-Opx}}$  and  $T_{\text{Ca-in-Opx}}$  formulations in the orthopyroxene core of this sample indicate that the anomalously low  $T_{\text{Cpx-Opx}}$  temperature may be the vestige of an older low-temperature event as reported in other xenolith suites (Foley et al., 2006). Egorova et al. (2006) ( $T_{\text{Ca-Opx}} = 1020$ – $1100$  °C) and Gibsher et al. (2008) ( $T_{\text{Ca-Opx}} = 970$ – $1100$  °C) have reported a similar range of equilibration temperatures for the Sangilen peridotite xenoliths.

Several studies have shown that the Sangilen lithospheric mantle records hotter geothermal regimes than the lithospheric mantle in nearby areas of the Siberian platform (Djomani et al., 2003; Khutorskoy and Yarmolyuk, 1989; Zorin et al., 1990). We hence assume that the paleogeothermal gradient of the Sangilen mantle is first approximated by a relatively hot geotherm as that derived from studies of spinel mantle xenoliths in intracontinental regions such as southeastern Australia (O'Reilly and Griffin, 1985). Calculated temperatures of Sangilen xenoliths plot along this geotherm at pressures ranging from 1.3 to 1.6 GPa, which correspond to lithospheric depths from  $\sim 43$  to 53 km (Fig. 5). This depth of provenance is in good agreement with the crustal thickness seismically imaged beneath the Sangilen plateau (Djomani et al., 2003; Khutorskoy and

**Table 1**

Average major element compositions (wt.%) of minerals, modal abundances and calculated equilibrium temperatures of the studied Sangilen xenoliths.

Sample	3H-2				3H-4				3H-8				5H-2			
	Spinel lherzolite coarse granular				Spinel lherzolite poikilitic				Spinel lherzolite poikilitic				Spinel lherzolite coarse equigranular			
Rock Texture																
Mineral	ol	opx	cpx	spl	ol	opx	cpx	spl	ol	opx	cpx	spl	ol	opx	cpx	spl
SiO <sub>2</sub>	40.9	55.8	53.1	0.07	40.7	54.2	51.5	0.15	40.5	53.7	51.0	0.06	40.0	54.1	51.3	0.06
TiO <sub>2</sub>	b.d.l.	0.05	0.13	0.22	b.d.l.	0.14	0.55	0.18	b.d.l.	0.18	0.59	0.19	b.d.l.	0.14	0.53	0.14
Al <sub>2</sub> O <sub>3</sub>	b.d.l.	2.79	3.49	29.4	b.d.l.	5.70	7.64	57.8	b.d.l.	5.20	7.03	55.6	b.d.l.	5.04	7.20	57.2
Cr <sub>2</sub> O <sub>3</sub>	b.d.l.	0.70	1.27	36.8	b.d.l.	0.42	0.73	9.07	b.d.l.	0.40	0.78	9.99	b.d.l.	0.39	0.84	10.3
FeO <sup>tot</sup>	9.86	6.21	3.06	16.1	10.2	6.48	3.43	10.9	10.8	6.92	3.57	11.9	10.27	6.58	3.33	11.1
MnO	0.13	0.12	0.09	0.12	0.15	0.13	0.10	0.11	0.13	0.15	0.09	0.10	0.18	0.18	0.13	0.22
MgO	48.8	32.5	16.9	16.0	47.2	31.1	15.0	20.2	48.2	31.4	15.0	20.2	48.8	32.6	15.8	20.7
NiO	0.32	0.09	b.d.l.	0.19	0.34	0.11	b.d.l.	0.36	0.33	0.12	b.d.l.	0.33	0.39	0.11	b.d.l.	0.39
CaO	0.09	1.08	19.6	b.d.l.	0.11	1.01	19.2	b.d.l.	0.09	0.962	18.9	b.d.l.	0.08	0.85	18.6	b.d.l.
Na <sub>2</sub> O	b.d.l.	0.08	0.87	b.d.l.	b.d.l.	0.15	1.67	b.d.l.	b.d.l.	0.15	1.69	b.d.l.	b.d.l.	0.14	1.75	b.d.l.
Total	100.2	99.4	98.5	99.0	98.8	99.4	99.9	98.7	100.1	99.2	98.7	98.3	99.8	100.1	99.6	100.1
mg#	89.8	90.3	90.7	63.9	89.2	89.5	89.9	78.2	88.9	89.0	88.3	74.6	89.4	89.9	89.5	77.0
cr#				45.7				9.52				10.7				10.8
vol.%	63.4	26.5	7.6	2.5	51.1	32.7	15.2	1.0	52.8	31.9	15.0	0.3	54.7	29.1	15.7	0.5
T <sub>Cpx-Opx</sub> (± 31 °C)	1096 °C				1031 °C				1019 °C				1042 °C			
T <sub>Ca-Opx</sub> (± 16 °C)	1075 °C				1060 °C				1047 °C				1014 °C			
T <sub>Ca-Opx-mod</sub> (± 25–45 °C)	1072 °C				1055 °C				1041 °C				1003 °C			
T <sub>Cr-Al-Opx</sub> (± 15 °C)	1020 °C				1038 °C				1009 °C				999 °C			

b.d.l. – below detection limit.

Using thermometers: TCpx-Opx – Taylor, 1998; TCa-Opx – Brey and Köhler, 1990; TCa-Opx-mod – Nimis and Grütter, 2010; TCr-Al-Opx – Witt-Eickschen and Seck, 1991.

Yarmolyuk, 1989; Zorin et al., 1990). Likewise, it is in good accordance with the spinel lherzolite nature of the Sangilen xenoliths, as the spinel-garnet peridotite transition at ~1000–1100 °C is approximately

located at 65 km (Fig. 5); significantly hotter or cooler paleo-geotherms would have resulted in equilibration of some xenoliths at plagioclase lherzolite or garnet lherzolite facies depths, respectively. These results are in good accordance with a Late Ordovician hot paleo-geothermal regime inferred for the Sangilen plateau that is similar to that recorded in younger, Neogene basalt-hosted spinel mantle xenoliths from the Baikal rift (Ionov, 2002).

In many suites of spinel peridotite xenoliths, samples with poikilitic texture usually record the highest equilibration temperatures and are commonly ascribed to recrystallization at near-solidus peridotite temperatures under high melt-rock ratios near the lithosphere–asthenosphere boundary (Embey-Isztin et al., 2001; Xu et al., 1998, 2003). The absence of correlation between equilibration temperature, textural and trace element types (Fig. 5) and the coincident high equilibration temperatures of Sangilen poikilitic xenoliths with those of other textural types point to the absence of a layered spatial distribution of the textural types in the sampled Sangilen lithospheric mantle.

## 6.2. Composition of the Sangilen Plateau lithospheric mantle: geochemical record of partial melting and metasomatism

### 6.2.1. The partial melting record

The spinel Cr# and olivine Mg# variations in Sangilen peridotite xenoliths indicate they are mostly residues of low to moderate (up to 10%) degrees of partial melting of a fertile peridotite mantle source (Fig. 3). Because clinopyroxene is the main carrier of trace elements in upper mantle anhydrous spinel peridotite (Garrido et al., 2000; McDonough and Frey, 1989; Rampone et al., 1991; Rivalenti et al., 1996; Stosch, 1982), its trace element composition is of particular interest to further constrain the magmatic processes that affected the Sangilen lithospheric mantle. The Yb<sub>N</sub> content of clinopyroxene is particularly a good proxy for depletion of mantle peridotite during spinel lherzolite facies melting because it mainly depends on the total melt extracted irrespectively of the melting mechanism (i.e., batch, fractional or incremental melting) (e.g., Johnson et al., 1990; Shaw, 1970) and it is hardly modified by post-melting processes associated with melt porous flow (Bodinier et al., 1988; Godard et al., 1995; Ionov et al., 2002; Lenoir et al., 2001; Ozawa and Shimizu, 1995; Soustelle et al., 2009; Suhr, 1999; Vernières et al., 1997). Fig. 6 displays the (Ce/Dy)<sub>N</sub> (Fig. 6a) and (Sm/Yb)<sub>N</sub> (Fig. 6b) versus the Yb<sub>N</sub> content of Sangilen peridotite clinopyroxenes and the variation of

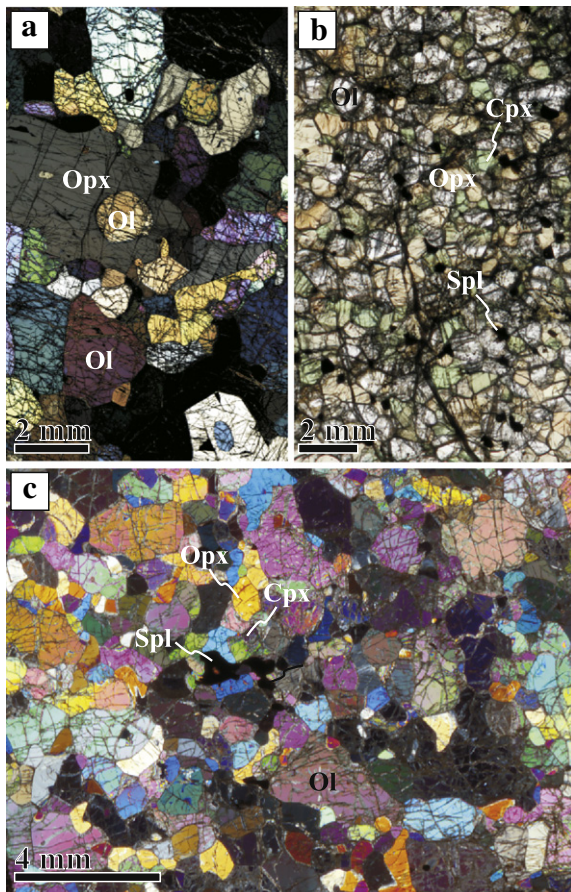


**Fig. 2.** Photomicrographs of representative textures of Sangilen mantle xenoliths: (a) poikilitic texture with olivine enclosed in large orthopyroxene (sample 5H-9); (b) coarse-grained equigranular texture with straight grain boundaries (sample 5H-2); (c) coarse granular texture with curvilinear grain boundaries (sample 3H-2). Cpx: clinopyroxene; Ol: olivine; Opx: orthopyroxene; Spl: spinel.

Table 1 (cont.)

5H-3				5H-7				5H-9				5H-10				5H-13			
Spinel lherzolite poikilitic				Spinel lherzolite poikilitic				Spinel lherzolite poikilitic				Spinel lherzolite coarse granular				Spinel lherzolite poikilitic			
ol	opx	cpx	spl	ol	opx	cpx	cpx	ol	opx	cpx	spl	ol	opx	cpx	spl	ol	opx	cpx	spl
40.5	53.8	51.8	0.06	40.7	55.0	52.7	0.05	40.3	54.6	51.7	0.05	41.1	54.9	52.0	0.12	40.9	56.2	53.2	0.06
b.d.l.	0.04	0.11	0.06	b.d.l.	0.07	0.23	0.08	b.d.l.	0.16	0.48	0.28	b.d.l.	0.11	0.31	0.21	b.d.l.	0.08	0.19	0.24
b.d.l.	4.64	5.52	50.2	b.d.l.	4.80	6.53	54.0	b.d.l.	4.68	6.03	48.7	b.d.l.	4.18	5.95	44.7	b.d.l.	2.88	3.95	31.1
b.d.l.	0.55	0.92	16.17	b.d.l.	0.53	1.03	14.43	b.d.l.	0.61	1.06	17.4	b.d.l.	0.63	1.38	22.82	b.d.l.	0.77	1.64	37.02
9.9	6.17	3.15	11.7	10.1	6.37	3.10	11.1	11.73	7.45	3.90	14.2	9.9	6.27	3.12	13.4	8.81	5.57	2.75	14.0
0.13	0.14	0.09	0.08	0.16	0.17	0.13	0.27	0.18	0.18	0.13	0.33	0.14	0.15	0.09	0.15	0.15	0.16	0.12	0.54
48.8	31.5	16.4	19.5	48.9	32.8	16.0	20.1	47.6	31.9	16.4	18.5	48.2	32.0	15.4	18.2	49.6	33.7	17.2	16.5
0.32	0.09	b.d.l.	0.28	0.39	0.10	b.d.l.	0.36	0.37	0.10	b.d.l.	0.31	0.36	0.10	b.d.l.	0.27	0.38	0.11	b.d.l.	0.20
0.10	1.09	20.0	b.d.l.	0.07	0.88	19.1	b.d.l.	0.09	1.03	19.0	b.d.l.	0.08	0.96	19.3	b.d.l.	0.08	0.96	19.8	b.d.l.
b.d.l.	0.10	0.92	b.d.l.	b.d.l.	0.13	1.59	b.d.l.	b.d.l.	0.09	1.19	b.d.l.	b.d.l.	0.15	1.61	b.d.l.	b.d.l.	0.08	1.14	b.d.l.
99.7	98.1	98.9	98.1	100.4	100.8	100.5	100.3	100.4	100.8	99.9	99.9	99.8	99.4	99.3	99.8	99.9	100.5	100.1	99.7
89.8	90.1	90.3	74.9	89.6	90.2	90.2	76.4	87.9	88.4	88.2	70.0	89.7	90.1	91.0	74.0	90.9	91.5	91.8	67.8
			17.8				15.2				19.4				25.5				44.4
65.5	20.1	13.4	1.1	68.4	20.7	9.8	1.1	72.6	20.9	6.3	0.2	81.5	11.2	6.9	0.4	82.5	10.9	6.1	0.5
1082 °C				1065 °C				1093 °C				847 °C				1063 °C			
1083 °C				1021 °C				1062 °C				1047 °C				1043 °C			
1081 °C				1012 °C				1057 °C				1041 °C				1037 °C			
1048 °C				1038 °C				1059 °C				1056 °C				1041 °C			

these parameters calculated for clinopyroxene in spinel peridotite residues of variable degrees of non-modal batch and fractional melting. In good accordance with their olivine and spinel compositions (Fig. 3), the Yb<sub>N</sub> content of clinopyroxene in xenoliths 3H4, 3H8 and 5H-2 records low degrees of partial melting (Fig. 6). The Yb<sub>N</sub> content of clinopyroxene in other Sangilen xenoliths indicates they are residues of up to ~40% batch melting or 15% fractional melting of a depleted mantle source; however, the lherzolite mineral assemblage of Sangilen xenoliths is more consistent with the lower melting degree estimates. The highest inferred melting degree corresponds to Type II 3H-2 and Type III 5H-13 xenoliths (Fig. 6), in good agreement with their highly

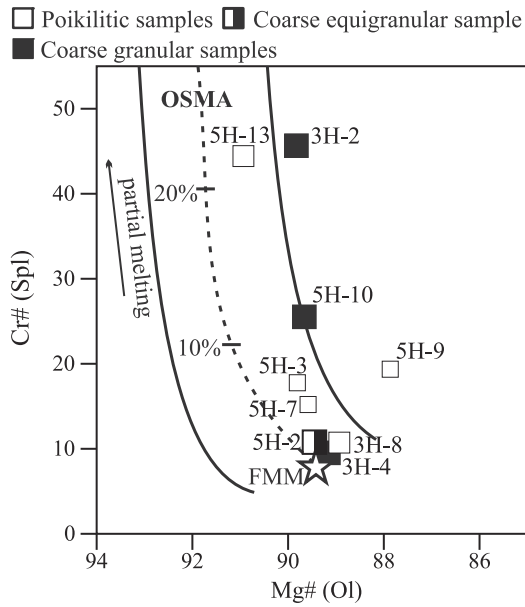
refractory spinel Cr# (Fig. 3). Only the elevated Yb<sub>N</sub> content of clinopyroxene in 5H-10 (Fig. 6) cannot be accounted for by partial melting from usual peridotite mantle sources and it most likely reflects enrichment by post-melting magmatic processes discussed below. So, partial melting alone cannot explain the REE variability of clinopyroxene in Sangilen mantle xenoliths (Fig. 6). Although the (Ce/Dy)<sub>N</sub> of clinopyroxene in Type I xenoliths 5H-7 and 5H-9 is consistent with being melting residues of variable degrees of batch melting (Fig. 6a), batch melting cannot reproduce their (Sm/Yb)<sub>N</sub> ratios (Fig. 6b). Furthermore, the (Ce/Dy)<sub>N</sub> ratio of clinopyroxene in xenoliths 3H-2, 5H-3 and 5H-13 is higher than that calculated for clinopyroxene residual of

Table 2

Average trace element abundances (ppm) of clinopyroxenes from the Sangilen xenoliths.

Sample	3H-2 (st. dev.)	3H-4 (st. dev.)	3H-8 (st. dev.)	5H-2 (st. dev.)	5H-3 (st. dev.)	5H-7 (st. dev.)	5H-9 (st. dev.)	5H-10 (st. dev.)	5H-13 (st. dev.)
Li	0.992	0.104		1.50	0.09	1.27	0.16	1.27	0.25
Rb	0.043	0.038	0.024	0.008	0.032	0.012	0.247	0.238	0.019
Th	0.039	2.1E-04	0.013	0.005	0.031	0.002	0.060	0.001	0.033
U	0.013	0.003	0.005	0.002	0.012	0.003	0.016	0.001	0.016
Nb	0.291	0.009	0.102	0.054	0.279	0.006	0.648	0.017	0.311
Ta	0.035	0.002	0.006	0.004	0.037	0.002	0.037	0.005	0.032
La	1.36	0.02	0.319	0.013	1.21	0.02	1.35	0.04	0.88
Ce	3.72	0.05	2.15	0.03	4.32	0.09	3.68	0.14	2.25
Pb	0.043	0.010	0.034	0.025	0.046	0.021	0.043	0.021	0.045
Sr	50.4	1.7	60.0	1.1	60.7	0.5	75.5	3.0	25.9
Pr	0.579	0.008	0.545	0.008	0.790	0.022	0.577	0.012	0.293
Nd	3.13	0.04	3.82	0.08	4.68	0.12	3.31	0.04	1.28
Hf	0.531	0.010	0.982	0.023	0.853	0.010	0.798	0.021	0.105
Zr	15.3	0.2	26.7	0.4	25.9	0.2	23.0	0.3	4.60
Sm	1.01	0.01	1.74	0.07	1.72	0.06	1.34	0.01	0.36
Eu	0.362	0.005	0.730	0.021	0.675	0.013	0.571	0.018	0.142
Gd	1.20	0.01	2.73	0.10	2.45	0.05	2.16	0.04	0.65
Tb	0.190	0.003	0.509	0.013	0.436	0.006	0.413	0.005	0.139
Ti	722	18	3788	25	3841	17	3067	178	955
Dy	1.16	0.01	3.79	0.09	3.11	0.04	3.04	0.05	1.20
Ho	0.223	0.002	0.805	0.028	0.666	0.011	0.672	0.013	0.285
Y	5.26	0.07	20.0	0.6	16.8	0.2	16.7	0.6	7.46
Er	0.559	0.008	2.35	0.07	1.92	0.02	1.93	0.06	0.896
Tm	0.074	0.001	0.338	0.010	0.274	0.004	0.281	0.007	0.141
Yb	0.448	0.006	2.21	0.07	1.79	0.03	1.81	0.06	0.950
Lu	0.065	0.002	0.314	0.009	0.253	0.004	0.265	0.009	0.143
(La/Sm) <sub>N</sub>	0.85		0.11		0.44		0.63		1.54
(La/Yb) <sub>N</sub>	2.06		0.10		0.46		0.51		0.63

The subscript N denotes chondrite-normalized element ratio (Sun and McDonough, 1989).



**Fig. 3.** Plot of spinel Cr# [100\*Cr/(Cr + Al)] versus olivine Mg# [100\*Mg/(Mg + Fe)]. The Olivine-Spinel Mantle Array (OSMA) and degrees of partial melting are from Arai (1994). FMM (open star) is the Fertile MORB Mantle after Pearce et al. (2000). Ol: olivine; Spl: spinel.

different melting mechanisms. These variations of  $(Ce/Dy)_N$  and  $(Sm/Yb)_N$  in clinopyroxene unexplained by melting most likely indicate that mantle xenoliths underwent post-melting modifications by metasomatism.

Irrespective of the melting mode, the depletion of Sangilen mantle xenoliths is not correlated either with textural type or their depth of provenance (cf. Figs. 5 & 6). Some cratonic and circumcratonic xenolith suites reveal compositionally and texturally layered lithospheric mantle related to different mechanisms of accretion of the continental and/or subducted lithosphere (e.g., Carlson et al., 2005; Foley et al., 2006; Griffin et al., 1999a, 2003, 2004; Pearson et al., 2007; Rudnick

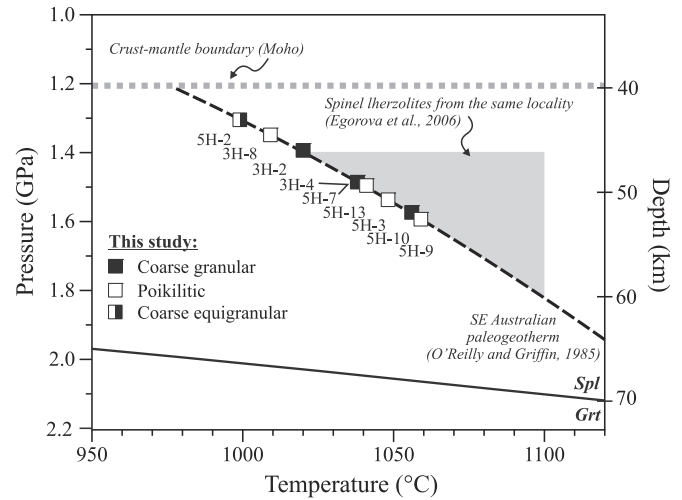


**Fig. 5.** Estimated equilibrium temperature of Sangilen spinel peridotites plotted along the SE Australia paleogeotherm (dashed black curve) (O'Reilly and Griffin, 1985). This paleogeotherm is taken as representative for intracontinental areas with high heat flow as suggested for the Sangilen plateau lithosphere at the time of intrusion of Ordovician Agardag lamprophyres. The spinel to garnet peridotite transition (solid black line) is calculated for a fertile lherzolite composition (O'Neill, 1981; Webb and Wood, 1986) and the crustal thickness (dashed gray line) is that of off-craton continental crust (Rudnick and Gao, 2003).

et al., 1993, 1998; Simon et al., 2007). The absence of layered structure in the sampled lithospheric mantle from the Sangilen plateau is instead consistent with growth by the succession of the accretionary tectonic processes associated with the building of the Tuva-Mongolia micro-continent (Djomani et al., 2003; Khutorsky and Yarmolyuk, 1989; Zorin et al., 1990).

#### 6.2.2. The mantle metasomatism record

Enrichments of incompatible trace elements relatively to predictions of partial melting models are commonly observed in mantle-derived peridotite (Bodinier and Godard, 2006; Downes, 2001; Hawkesworth

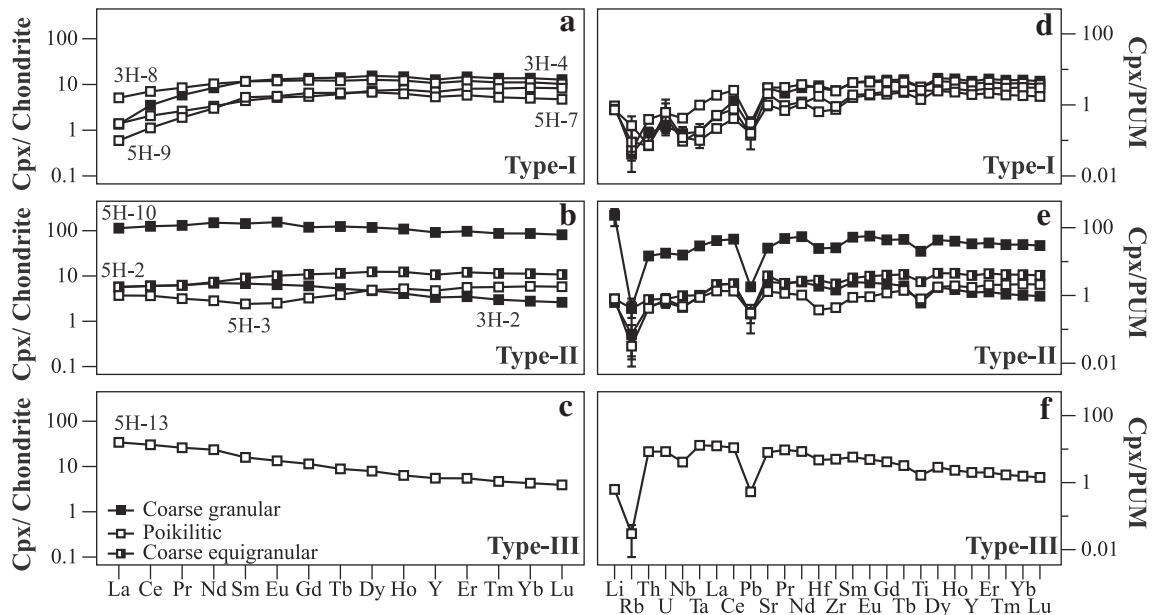


**Fig. 4.** Geochemical classification of Sangilen spinel peridotite xenoliths based on C1 chondrite-normalized REE patterns (a–c) and Primitive Upper Mantle (PUM) normalized trace element patterns (d–f) of clinopyroxenes (see text for further details). Reported values are the average composition of several clinopyroxene analyses per sample ( $n > 6$ ). Error bars in panels d–f are 2 SD (standard deviation) only shown for analyses where the relative error is larger than 10%. Normalizing values after Sun and McDonough (1989).

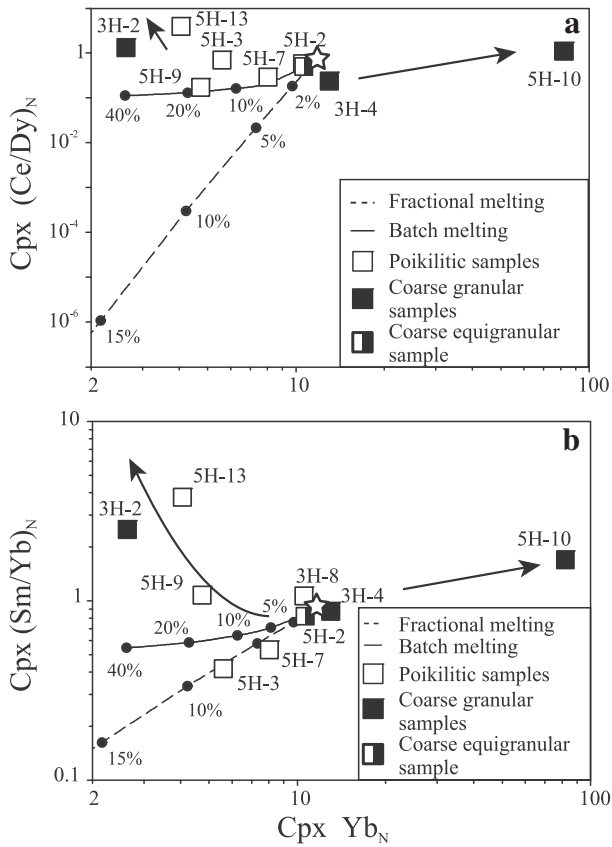


**Fig. 6.**  $Yb_N$  contents versus  $(Ce/Dy)_N$  (a) and  $(Sm/Yb)_N$  (b) of clinopyroxene ( $N =$  chondrite-normalized after Sun and McDonough, 1989) in Sangilen Plateau mantle xenoliths compared with those of spinel peridotite residues of non-modal fractional (dashed lines) and batch (solid curves) melting of depleted MORB mantle (open star) (Salters and Stracke, 2004). The source and melting modal proportions (ol:opx:cpx) are taken for peridotite melting at 2 GPa after Niu (1997) and are, respectively, 0.57:0.28:0.15 and  $-0.03:0.50:0.53$ . Number labels in melting curves indicate degrees of partial melting. The bulk composition partition coefficients are taken from Bedini et al. (1997) and Su et al. (2003). Black arrows indicate variations that cannot be accounted for by melting models and are most likely due to post-melting, mantle metasomatism (see text for further details).

et al., 1984; Pearson et al., 2003; and references therein). These compositional modifications, which are collectively referred to as mantle metasomatism (Menzies and Hawkesworth, 1987a; and references therein),

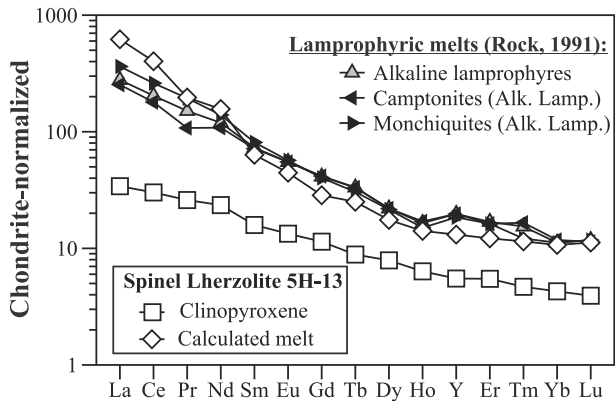


**Fig. 7.** C1 chondrite-normalized REE patterns of clinopyroxene (open squares) of Sangilen xenolith 5H-13 and the calculated melt (open diamonds; partition coefficients from McKenzie and O’Nions, 1991) in exchange equilibrium with it compared with the REE patterns of common alkaline lamprophyres (after Rock, 1991). Normalizing values after Sun and McDonough (1989).

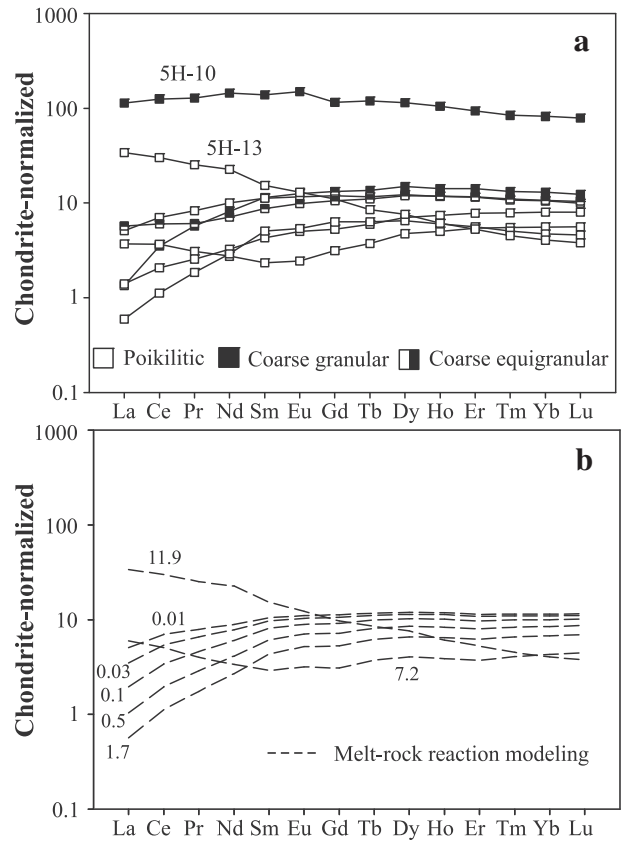


**Fig. 8.** C1 Chondrite normalized REE patterns of clinopyroxene in the Sangilen spinel lherzolite (a) (symbols as in Fig. 3) compared with (b) those for clinopyroxene obtained from modeling of melt-peridotite reaction using the plate model of Vernières et al. (1997) for the simulation of the trace element fractionation during partial melting and magma transport in the upper mantle. The REE composition of the melt reacting with mantle peridotite is that in equilibrium with clinopyroxene sample 5H-13 (see Fig. 7). The REE and modal compositions of the peridotite source are those of the depleted MORB mantle (Salters and Stracke, 2004). The melt-rock reaction used in the simulation is:  $0.9 \text{ Opx} + 0.45 \text{ Cpx} = 0.35 \text{ Ol} + 1 \text{ Melt}$ . The number of reaction cells and dissolution increment (Vernières et al., 1997) are, respectively, 100 and 0.0024. The curve shows the best fits to clinopyroxene compositions of all Sangilen xenoliths (Fig. 8b) but sample 5H-10; labels on dashed patterns indicate the instantaneous melt/rock ratio. Partition coefficients are from Bedini et al. (1997) and Su et al. (2003). Normalizing values after Sun and McDonough (1989).

are generally ascribed to post-melting magmatic processes caused by melt/rock reactions involving percolation of small fractions of fluids, volatile-rich silicate melts and/or carbonate melts through asthenospheric or lithospheric mantle (e.g., Bell et al., 2005; Bodinier et al., 1990; Dautria et al., 1992; Garrido and Bodinier, 1999; Gregoire et al., 2001; Harte et al., 1993; Ionov et al., 2002; Lenoir et al., 2001; McKenzie, 1989; Soustelle et al., 2009). Transient chromatographic chemical fractionation produced by metasomatic melts/fluids percolating through a peridotite matrix may account for the variable fractionation of LREE-MREE relative to HREE observed in Sangilen xenoliths (Fig. 6). According to the chromatographic fractionation model, porous flow of melt/fluid through peridotite generates chromatographic fronts for trace elements of different compatibility; accordingly, LREE chromatographic fronts travel significantly faster than those of more compatible MREE and HREE. This dynamic chemical fractionation creates transient enrichment of incompatible elements in both the percolated peridotite and the metasomatic melt (Bodinier et al., 1990; Godard et al., 1995; Navon and Stolper, 1987; Soustelle et al., 2009; Takazawa et al., 1992; Vernières et al., 1997). For a constant integrated melt/rock ratio and absence of mineralogical reaction, peridotite affected by the highest melt/rock ratio are in closer trace element exchange equilibrium

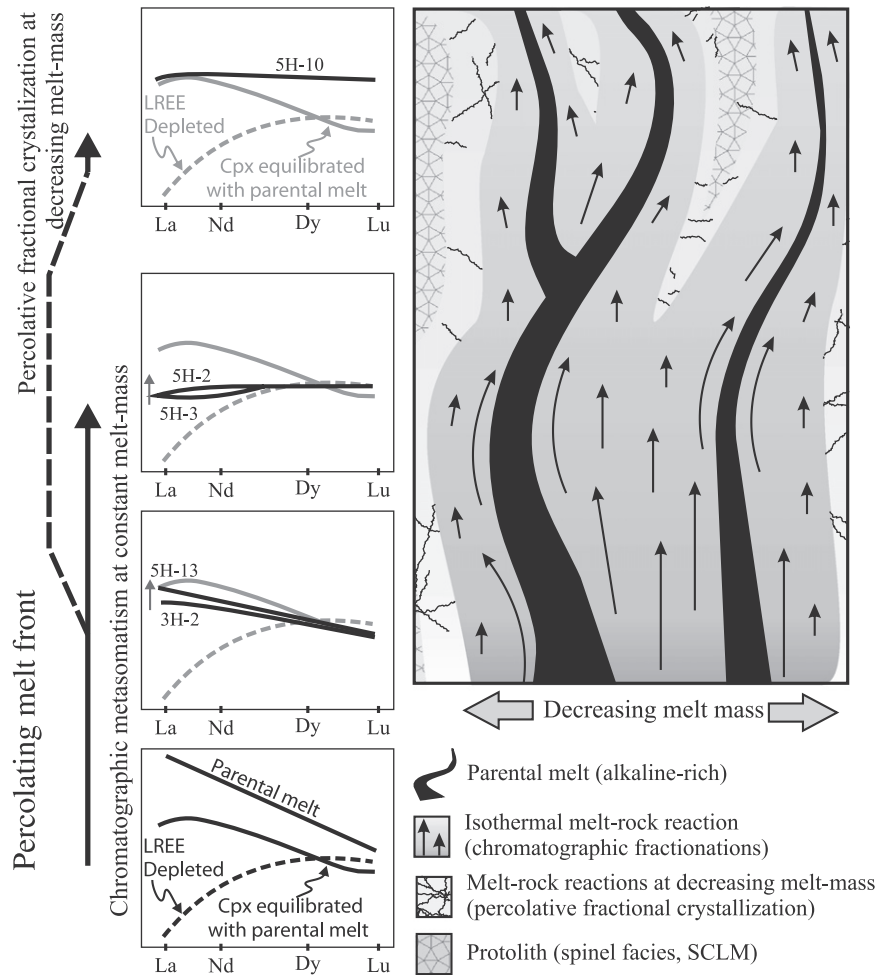


**Fig. 9.** Cartoon of conceptual model (right panel) to account for the trace element variability of Sangilen plateau peridotite xenoliths by mantle metasomatism produced by a veined network of parental alkaline-rich melts reacting with variable depleted source lithospheric peridotites. See text for further details.

with the primordial metasomatic melt (Navon and Stolper, 1987; Vasseur et al., 1991; Vernières et al., 1997).

A potential candidate for unraveling the trace element composition of the parental metasomatic agent in Sangilen peridotites is Type III xenolith 5H-13. The LREE-enriched normalized pattern of clinopyroxene in this sample (Fig. 4c) is in trace element exchange equilibrium with mantle-derived alkaline melts (Fig. 7). Several studies have reported genetic links between alkali basalts and precursor metasomatic agents that metasomatized their hosted spinel mantle xenoliths (Bedini et al., 1997; Dautria et al., 1992; Downes, 2001); it is hence conceivable that the Sangilen mantle was metasomatized by alkaline melts similar – or precursor – to the Agardag lamprophyres. Carbonate melts are also extremely rich in incompatible trace elements and effective metasomatic agents due to their capability of easily migrating through peridotite owing to low melt–solid dihedral angles (Dautria et al., 1992; Ionov et al., 1993; Rudnick et al., 1993; Watson and Brenan, 1987; Yaxley et al., 1991). Although clinopyroxene in some Types II and III Sangilen xenoliths is LREE-enriched (Fig. 4b–c), it lacks the trace element signature that characterizes peridotite clinopyroxene metasomatized by carbonate melts; namely, negative anomalies of high field strength elements (Ti, Nb, Ta, Zr and Hf) relative to REE and Th–U, and low Ti/Eu ratios (Fig. 4 e–f) (Coltorti et al., 1999; Dautria et al., 1992; Foley et al., 2009; Gregoire et al., 2000; Ionov et al., 1993; Klemme et al., 1995; Rudnick et al., 1993). Although the

physical nature of the metasomatic agent that affected Sangilen xenoliths remains mostly unconstrained, trace element variations in clinopyroxene suggest that it was alkaline silicate melt, similarly to spinel peridotite xenoliths from West Eifel (Zinngrebe and Foley, 1995).

Fig. 8 shows the results of melt/rock reaction simulation using the plate numerical model of Vernières et al. (1997) aiming to test whether variable REE patterns of clinopyroxene in Sangilen xenoliths (Fig. 4a–c) may be reproduced by reaction between depleted peridotite and a percolating alkaline melt in equilibrium with the clinopyroxene of 5H-13 (Type III sample in Fig. 4c) as shown in Fig. 7. Modeling results show that clinopyroxene REE patterns of Sangilen xenoliths (Fig. 8a) can be reproduced satisfactorily by variable integrated melt/peridotite ratios and constant melt mass of a LREE-rich alkaline parental melt percolating through a depleted lithospheric peridotite (Fig. 8b). Only the clinopyroxene composition of 5H-10 cannot be ascribed to the percolation metasomatic model described above, as its trace element contents are too high (Fig. 8a). In a melt–peridotite percolation scenario, such high concentrations can be explained by percolation of the same parental metasomatic melt coupled with fractional crystallization and reaction with host peridotites at decreasing melt mass (the percolative fractional crystallization model of Harte et al., 1993). As reported for other mantle spinel peridotites, percolation of metasomatic melts reacting with host peridotite at decreasing melt–rock ratios causes substantial enrichment of trace elements

(Bedini et al., 1997; Bodinier et al., 2008; Soustelle et al., 2009) and may account for their high contents in clinopyroxene in 5H-10 (Fig. 4e).

Fig. 9 gives a portrait of a conceptual model for metasomatism by alkaline melts in the Sangilen lithospheric mantle. As for melting-induced compositional variations, trace element variations due to metasomatism in Sangilen xenoliths are not correlated with the xenolith textural type and equilibration temperature and, therefore, depth of provenance (cf. Figs. 4, 5 & 8). In contrast with other subcontinental lithospheric mantle sections, where correlation between texture and equilibration temperature of spinel peridotite xenoliths reveals systematic variations of metasomatic reactions with depth at lithospheric length scales (Bedini et al., 1997), Sangilen xenoliths seem to reveal a more heterogeneous metasomatic imprint that may be better explained by variable, vein-related reactions throughout the lithospheric section (Bodinier et al., 1990, 2004; Harte et al., 1993; Wilshire, 1987) (Fig. 9). The absence in Sangilen xenoliths of hydrous minerals distinctive of modal metasomatism, such as amphibole or phlogopite, indicates incompatible trace element enrichments were generated by cryptic metasomatism (Harte et al., 1993; Hawkesworth et al., 1984; Menzies and Hawkesworth, 1987a, 1987b). As hydrous minerals are common liquidus phases in alkaline mafic magmas and lamprophyres at depth of equilibration of spinel peridotites (Foley, 1984, 1990; Foley et al., 2009), cryptic metasomatism further constrains metasomatism at elevated temperature that can only be accounted in the wall rock of veins where super solidus alkaline melt circulated. Near-isothermal, melt-peridotite metasomatic reactions at constant melt mass (Figs. 8 & 9 right panel) along wall peridotite of intrusive dikes may be responsible for variable REE variations observed in clinopyroxenes from Sangilen xenoliths (Fig. 9). Further crystallization of metasomatic melts at decreasing temperature away from dykes would result in over-enrichment of trace elements in metasomatized peridotite as seen in sample 5H-10 (Fig. 9 left panel). Far from intrusive dykes, lithospheric mantle section is characterized by depleted mantle composition. If melt intrusion occurred at temperature above the stability of hydrous phases in the metasomatic alkaline melts, once the magmatic activity ceased no trace of metasomatism would remain other than its cryptic imprint.

## 7. Conclusions

On the basis of our petrological and geochemical study of Sangilen mantle xenoliths, the following conclusions can be drawn:

- i. Sangilen xenoliths record a narrow range of equilibration temperature (ca. 1000–1100 °C) plotting along a relatively hot intracontinental geotherm at lithospheric depths from ~43 to 53 km (1.3 to 1.6 GPa).
- ii. Their variation of olivine Mg# (87.9–90.9) with spinel Cr# (9.5–45.7) indicates xenoliths are mostly residues of up to 10% melting of a depleted peridotite source.
- iii. The elevated Yb<sub>N</sub> content of clinopyroxene in sample 5H-10 and the variable fractionation of LREE-MREE relative to HREE in clinopyroxene from other xenoliths indicate they underwent variable metasomatic processes. These processes probably consisted of episodes of percolation-reaction through peridotite of small-melt fractions of alkaline mafic melts precursor to Agardag alkaline lamprophyres.
- iv. The lack of correlation with depth of modal variations, textural types, inferred degrees of melting and trace element patterns of clinopyroxene indicates the absence of a texturally or compositionally layering in the lithospheric mantle beneath the Sangilen plateau sampled by Ordovician lamprophyres. The observed compositionally variation of xenoliths is better accounted by depleted lithosphere variably metasomatized along a network of percolating alkaline mafic melts heterogeneously distributed throughout the Sangilen lithospheric mantle section.

## Acknowledgments

The authors appreciate the editorial work of Dr. Andrew Kerr and the constructive comments of Dr. Michel Grégoire and an anonymous reviewer. M. R. Reyes-González is thanked for supplying high quality polished thin sections and sample preparation. We acknowledge funding from the “Ministerio de Economía y Competitividad” (Grant CGL2010-14848), the “Junta de Andalucía” (research group RNM-131 and grant 2009RNM4495), the International Lithosphere Program (ILP) (CC4-MEDYNA) and the Joint Research of the Russian Academy of Sciences and the Hungarian Academy of Sciences (project #55 to C. Szabó). Z. Konc’s Ph.D research is supported by a CSIC JAE-PreDoc fellowship (2008JAEPre033). This research has been funded partially by the European Fund for Regional Development.

## References

- Arai, S., 1994. Compositional variation of olivine-chromian spinel in Mg-rich magmas as a guide to their residual spinel peridotites. *Journal of Volcanology and Geothermal Research* 59, 279–293.
- Bedini, R.M., Bodinier, J.L., Dautria, J.M., Morten, L., 1997. Evolution of LILE-enriched small melt fractions in the lithospheric mantle: a case study from the East African Rift. *Earth and Planetary Science Letters* 153, 67–83.
- Bell, D.R., Gregoire, M., Grove, T.L., Chatterjee, N., Carlson, R.W., Buseck, P.R., 2005. Silica and volatile-element metasomatism of Archean mantle: a xenolith-scale example from the Kaapvaal Craton. *Contributions to Mineralogy and Petrology* 150, 251–267.
- Berzin, N.A., Coleman, R.G., Dobretsov, N.L., Zonenshain, L.P., Xiao, X., Chang, E., 1994. Geodynamic map of the western part of Paleosian ocean. *Russian Geology and Geophysics* 35, 5–52.
- Bodinier, J.L., Godard, M., 2006. Orogenic, Ophiolitic and Abyssal Peridotites. In: Carlson, R.W. (Ed.), *Treatise on Geochemistry: Geochemistry of the Mantle and Core*, 2. Elsevier.
- Bodinier, J.L., Dupuy, C., Vernières, J., 1988. Behavior of trace-elements during upper mantle metasomatism – evidences from the Lherz massif. *Chemical Geology* 70, 152–152.
- Bodinier, J.L., Vasseur, G., Vernières, J., Dupuy, C., Fabries, J., 1990. Mechanisms of mantle metasomatism: geochemical evidence from the Lherz orogenic peridotite. *Journal of Petrology* 31, 597–628.
- Bodinier, J.L., Menzies, M.A., Shimizu, N., Frey, F.A., McPherson, E., 2004. Silicate, hydrous and carbonate metasomatism at Lherz, France: contemporaneous derivatives of silicate melt-harzburgite reaction. *Journal of Petrology* 45, 299–320.
- Bodinier, J.L., Garrido, C.J., Chanéfo, I., Bruguier, O., Gervilla, F., 2008. Origin of pyroxenite-peridotite veined mantle by refertilization reactions: evidence from the Ronda peridotite (Southern Spain). *Journal of Petrology* 49, 999–1025.
- Brey, G.P., Köhler, T., 1990. Geothermobarometry in four-phase lherzolites. II. New thermobarometers, and practical assessment of existing thermobarometers. *Journal of Petrology* 31, 1353–1378.
- Carlson, R.W., Pearson, D.G., James, D.E., 2005. Physical, chemical, and chronological characteristics of continental mantle. *Reviews of Geophysics* 43 (Art. n° 2004RG000156).
- Coltorti, M., Bonadiman, C., Hinton, R.W., Siena, F., Upton, B.G.J., 1999. Carbonatite metasomatism of the oceanic upper mantle: evidence from clinopyroxenes and glasses in ultramafic xenoliths of Grande Comore, Indian Ocean. *Journal of Petrology* 40, 133–165.
- Dautria, J.M., Dupuy, C., Takherist, D., Dostal, J., 1992. Carbonate metasomatism in the lithospheric mantle: peridotite xenoliths from a melilititic district of the Sahara basin. *Contributions to Mineralogy and Petrology* 111, 37–52.
- Djomani, Y.H.P., O’Reilly, S.Y., Griffin, W.L., Natapov, L.M., Erinchev, Y., Hronsky, J., 2003. Upper mantle structure beneath eastern Siberia: evidence from gravity modeling and mantle petrology. *Geochemistry, Geophysics, Geosystems* 4 (art. no.-1066).
- Dobretsov, N.L., Buslov, M.M., 2007. Late Cambrian-Ordovician tectonics and geodynamics of Central Asia. *Russian Geology and Geophysics* 48, 71–82.
- Downes, H., 2001. Formation and modification of the shallow sub-continental lithospheric mantle: a review of geochemical evidence from ultramafic xenolith suites and tectonically emplaced ultramafic massifs of western and central Europe. *Journal of Petrology* 42, 233–250.
- Downes, H., Embeyisztn, A., Thirlwall, M.F., 1992. Petrology and geochemistry of spinel peridotite xenoliths from the western Pannonian Basin (Hungary) – evidence for an association between enrichment and texture in the upper Mantle. *Contributions to Mineralogy and Petrology* 109, 340–354.
- Egorova, V.V., Volkova, N.I., Shelepaev, R.A., Izokh, A.E., 2006. The lithosphere beneath the Sangilen Plateau, Siberia: evidence from peridotite, pyroxenite and gabbro xenoliths from alkaline basalts. *Mineralogy and Petrology* 88, 419–441.
- Embeyisztn, A., Dobosi, G., Altherr, R., Meyer, H.P., 2001. Thermal evolution of the lithosphere beneath the western Pannonian Basin: evidence from deep-seated xenoliths. *Tectonophysics* 331, 285–306.
- Foley, S.F., 1984. Liquid immiscibility and melt segregation in alkaline lamprophyres from Labrador. *Lithos* 17, 127–137.
- Foley, S.F., 1990. A review and assessment of experiments on kimberlites, lamproites and lamprophyres as a guide to their origin. *Proceedings of the Indian Academy of Sciences Earth and Planetary Sciences* 99, 57–80.

- Foley, S.F., Andronikov, A.V., Jacob, D.E., Melzer, S., 2006. Evidence from Antarctic mantle peridotite xenoliths for changes in mineralogy, geochemistry and geothermal gradients beneath a developing rift. *Geochimica et Cosmochimica Acta* 70, 3096–3120.
- Foley, S.F., Yaxley, G.M., Rosenthal, A., Buhre, S., Kiseeva, E.S., Rapp, R.P., Jacob, D.E., 2009. The composition of near-solidus melts of peridotite in the presence of CO<sub>2</sub> and H<sub>2</sub>O between 40 and 60 kbar. *Lithos* 112, 274–283.
- Garrido, C.J., Bodinier, J.L., 1999. Diversity of mafic rocks in the Ronda peridotite: evidence for pervasive melt-rock reaction during heating of subcontinental lithosphere by upwelling asthenosphere. *Journal of Petrology* 40, 729–754.
- Garrido, C.J., Bodinier, J.L., Alard, O., 2000. Incompatible trace element partitioning and residence in anhydrous spinel peridotites and websterites from the Ronda orogenic peridotite. *Earth and Planetary Science Letters* 181, 341–358.
- Gibsher, A., Malkovets, V., Litasov, Y., Griffin, W., O'Reilly, S., 2008. An evidence for the composition of the Ordovician upper mantle beneath West Sangilen (Southeast Tuva, Russia). An evidence for the composition of the Ordovician upper mantle beneath West Sangilen (Southeast Tuva, Russia). *Frankfurt (Germany)*, p. A-00153.
- Gibsher, A.A., Malkovets, V.G., Travin, A.V., Belousova, E.A., Sharygin, V.V., Konc, Z., 2012. The age of camptonite dikes of the Agardag alkali-basalt complex (western Sangilen): results of Ar/Ar and U/Pb dating. *Russian Geology and Geophysics* 53, 998–1013.
- Godard, M., Bodinier, J.L., Vasseur, G., 1995. Effects of mineralogical reactions on trace-element redistributions in mantle rocks during percolation processes – a chromatographic approach. *Earth and Planetary Science Letters* 133, 449–461.
- Gregoire, M., Lorand, J.P., Cottin, J.Y., Giret, A., Mattielli, N., Weis, D., 1997. Xenoliths evidence for a refractory oceanic mantle percolated by basaltic melts beneath the Kerguelen archipelago. *European Journal of Mineralogy* 9, 1085–1100.
- Gregoire, M., Moine, B.N., O'Reilly, S.Y., Cottin, J.Y., Giret, A., 2000. Trace element residence and partitioning in mantle xenoliths metasomatized by highly alkaline, silicate- and carbonate-rich melts (Kerguelen Islands, Indian Ocean). *Journal of Petrology* 41, 477–509.
- Gregoire, M., McInnes, B.I.A., O'Reilly, S.Y., 2001. Hydrous metasomatism of oceanic sub-arc mantle, Lihir, Papua New Guinea – Part 2. Trace element characteristics of slab-derived fluids. *Lithos* 59, 91–108.
- Griffin, W.L., Doyle, B.J., Ryan, C.G., Pearson, N.J., O'Reilly, S.Y., Davies, R., Kivi, K., Van Achtebergh, E., Natapov, L.M., 1999a. Layered mantle lithosphere in the Lac de Gras area, Slave Craton: composition, structure and origin. *Journal of Petrology* 40, 705–727.
- Griffin, W.L., Ryan, C.G., Kaminsky, F.V., O'Reilly, S.Y., Natapov, L.M., Win, T.T., Kinny, P.D., Ilupin, I.P., 1999b. The Siberian lithosphere traverse: mantle terranes and the assembly of the Siberian Craton. *Tectonophysics* 310, 1–35.
- Griffin, W.L., O'Reilly, S.Y., Natapov, L.M., Ryan, C.G., 2003. The evolution of lithospheric mantle beneath the Kalahari Craton and its margins. *Lithos* 71, 215–241.
- Griffin, W.L., O'Reilly, S.Y., Doyle, B.J., Pearson, N.J., Coopersmith, H., Kivi, K., Malkovets, V., Pokhilenko, N., 2004. Lithosphere mapping beneath the north American plate. *Lithos* 77, 873–922.
- Harte, B., Hunter, R.H., Kinny, P.D., 1993. Melt geometry, movement and crystallization, in relation to mantle dykes, veins and metasomatism. *Philosophical Transactions: Physical Sciences and Engineering* 342, 1–21.
- Hawkesworth, C.J., Rogers, N.W., Vancalsteren, P.W.C., Menzies, M.A., 1984. Mantle enrichment processes. *Nature* 311, 331–335.
- Ilyin, A.V., 1990. Proterozoic supercontinent, its latest Precambrian rifting, breakup, dispersal into smaller continents, and subsidence of their margins: evidence from Asia. *Geology* 18, 1231–1234.
- Ionov, D., 2002. Mantle structure and rifting processes in the Baikal-Mongolia region: geophysical data and evidence from xenoliths in volcanic rocks. *Tectonophysics* 351, 41–60.
- Ionov, D.A., Dupuy, C., O'Reilly, S.Y., Kopylova, M.G., Genshaft, Y.S., 1993. Carbonated peridotite xenoliths from Spitsbergen – implications for trace-element signature of mantle carbonate metasomatism. *Earth and Planetary Science Letters* 119, 283–297.
- Ionov, D.A., Bodinier, J.L., Mukasa, S.B., Zanetti, A., 2002. Mechanisms and sources of mantle metasomatism: major and trace element compositions of peridotite xenoliths from Spitsbergen in the context of numerical modelling. *Journal of Petrology* 43, 2219–2259.
- Izokh, A.E., Polyakov, G.V., Mal'kovets, V.G., Shelepae, R.A., Travin, A.V., Litasov, Y.D., Gibsher, A.A., 2001. The Late Ordovician age of camptonites from the Agardag Complex of southeastern Tuva as an indicator of the plume-related magmatism during collision processes. *Doklady Earth Sciences* 379, 511–514.
- Johnson, K.T.M., Dick, H.J.B., Shimizu, N., 1990. Melting in the oceanic upper mantle: an ion microprobe study of diopsides in abyssal peridotites. *Journal of Geophysical Research* 95, 2661–2678.
- Khutorskoy, M.D., Yarmolyuk, V.V., 1989. Thermal and magmatic evolution of the lithosphere of Mongolia. *International Geology Review* 31, 1084–1096.
- Klemme, S., Vanderlaan, S.R., Foley, S.F., Gunther, D., 1995. Experimentally determined trace and minor element partitioning between clinopyroxene and carbonatite melt under upper-mantle conditions. *Earth and Planetary Science Letters* 133, 439–448.
- Lenoir, X., Garrido, C.J., Bodinier, J.L., Dautria, J.M., 2000. Contrasting lithospheric mantle domains beneath the Massif Central (France) revealed by geochemistry of peridotite xenoliths. *Earth and Planetary Science Letters* 181, 359–375.
- Lenoir, X., Garrido, C.J., Bodinier, J.L., Dautria, J.M., Gervilla, F., 2001. The recrystallization front of the Ronda peridotite: evidence for melting and thermal erosion of subcontinental lithospheric mantle beneath the Alboran basin. *Journal of Petrology* 42, 141–158.
- Litasov, K.D., Foley, S.F., Litasov, Y.D., 2000. Magmatic modification and metasomatism of the subcontinental mantle beneath the Vitim volcanic field (East Siberia): evidence from trace element data on pyroxenite and peridotite xenoliths from Miocene picrobasalt. *Lithos* 54, 83–114.
- Maaloe, S., Aoki, K.I., 1977. Major element composition of upper mantle estimated from composition of lherzolites. *Contributions To Mineralogy And Petrology* 63, 161–173.
- McDonough, W.F., Frey, F.A., 1989. Rare earth elements in upper mantle rocks. In: Lipin, B.R., McKay, G.A. (Eds.), *Geochemistry and Mineralogy of Rare Earth Elements*. Mineralogical Society of America, Washington D.C., pp. 99–145.
- McKenzie, D., 1989. Some remarks on the movement of small melt fractions in the mantle. *Earth and Planetary Science Letters* 95, 53–72.
- McKenzie, D., O'Nions, R.K., 1991. Partial melt distributions from inversion of rare earth element concentrations. *Journal of Petrology* 32, 1021–1091.
- Menzies, M.A., Hawkesworth, C.J., 1987a. *Mantle Metasomatism, Mantle Metasomatism*. Academic Press, London, p. 472.
- Menzies, M.A., Hawkesworth, C.J., 1987b. Upper mantle processes and composition. In: Nixon, P.H. (Ed.), *Mantle Xenoliths*. John Wiley & Sons, Chichester, United Kingdom, pp. 725–738.
- Mercier, J.C.C., Nicolas, A., 1975. Textures and fabrics of upper-mantle peridotites as illustrated by xenoliths from basalts. *Journal of Petrology* 16, 454–487.
- Mossakovskii, A.A., Ruzhentsev, S.V., Samygin, S.G., Kheraskova, T.N., 1993. Central Asian fold belt: geodynamic evolution and history of formation. *Geotectonics* 6, 3–33.
- Navon, O., Stolper, E., 1987. Geochemical consequence of melt percolation: the upper mantle as a chromatographic column. *Journal of Geology* 95, 285–307.
- Nimis, P., Grütter, H., 2010. Internally consistent geothermometers for garnet peridotites and pyroxenites. *Contributions to Mineralogy and Petrology* 159, 411–427.
- Niu, Y., 1997. Mantle melting and melt extraction processes beneath ocean ridges: evidence from abyssal peridotites. *Journal of Petrology* 38, 1047–1074.
- O'Neill, H.St C., 1981. The transition between spinel lherzolite and garnet lherzolite, and its use as a geobarometer. *Contributions to Mineralogy and Petrology* 77, 185–194.
- O'Reilly, S.Y., Griffin, W.L., 1985. A xenolith-derived geotherm for southeastern Australia and its geophysical implications. *Tectonophysics* 111, 41–63.
- Ozawa, K., Shimizu, N., 1995. Open system melting in the upper-mantle – constraints from the Hayachine-Miyamori ophiolite, Northeastern Japan. *Journal of Geophysical Research* 100, 22315–22335.
- Pearce, N.J.G., Perkins, W.T., Westgate, J.A., Gorton, M.P., Jackson, S.E., Neal, C.R., Chener, S.P., 1997. A compilation of new and published major and trace element data for NIST SRM 610 and NIST SRM 612 glass reference materials. *Geostandards Newsletter* 21, 115–144.
- Pearce, J.A., Barker, P.F., Edwards, S.J., Parkinson, I.J., Leat, P.T., 2000. Geochemistry and tectonic significance of peridotites from the South Sandwich arc-basin system, South Atlantic. *Contributions to Mineralogy and Petrology* 139, 36–53.
- Pearson, D.G., Canil, D., Shirey, S.B., 2003. Mantle Samples Included in Volcanic Rocks: Xenoliths and Diamonds. In: Carlson, R.W. (Ed.), *Treatise on Geochemistry: Geochemistry of the Mantle and Core*, 2. Elsevier.
- Pearson, D.G., Parman, S.W., Nowell, G.M., 2007. A link between large mantle melting events and continent growth seen in osmium isotopes. *Nature* 449, 202–205.
- Rampone, E., Bottazzi, P., Ottolini, L., 1991. Complementary Ti and Zr anomalies in orthopyroxene and clinopyroxene from mantle peridotites. *Nature* 354, 518–520.
- Rivalenti, G., Vannucci, R., Rampone, E., Mazzucchelli, M., Piccardo, G.B., Piccirillo, E.M., Bottazzi, P., Ottolini, L., 1996. Peridotite clinopyroxene chemistry reflects mantle processes rather than continental versus oceanic settings. *Earth and Planetary Science Letters* 139, 423–437.
- Rock, N.M.S., 1991. *Lamprophyres*. Van Nostrand Reinhold, New York.
- Rudnick, R.L., Gao, S., 2003. Composition of the Continental Crust. In: Rudnick, R.L. (Ed.), *Treatise on Geochemistry: Geochemistry of the Crust*. Elsevier, pp. 1–64.
- Rudnick, R.L., McDonough, W.F., Chappell, B.W., 1993. Carbonatite metasomatism in the northern Tanzanian mantle – petrographic and geochemical characteristics. *Earth and Planetary Science Letters* 114, 463–475.
- Rudnick, R.L., McDonough, W.F., O'Connell, R.J., 1998. Thermal structure, thickness and composition of continental lithosphere. *Chemical Geology* 145, 395–411.
- Salter, V.J.M., Stracke, A., 2004. Composition of the depleted mantle. *Geochemistry, Geophysics, Geosystems* 5, Q05B07.
- Shaw, D.M., 1970. Trace element fractionation during anatexis. *Geochimica et Cosmochimica Acta* 34, 237–243.
- Simon, N.S.C., Carlson, R.W., Pearson, D.G., Davies, G.R., 2007. The origin and evolution of the Kaapvaal cratonic lithospheric mantle. *Journal of Petrology* 48, 589–625.
- Soustelle, V., Tommasi, A., Bodinier, J.L., Garrido, C.J., Vauchez, A., 2009. Deformation and reactive melt transport in the mantle lithosphere above a large-scale partial melting domain: the Ronda peridotite massif, Southern Spain. *Journal of Petrology* 50, 1235–1266.
- Stosch, H.-G., 1982. Rare earth element partitioning between minerals from anhydrous spinel peridotite xenoliths. *Geochimica et Cosmochimica Acta* 46, 793–881.
- Su, Y.J., Langmuir, C.H., Asimow, P.D., 2003. PetroPlot: a plotting and data management tool set for Microsoft Excel. *Geochemistry, Geophysics, Geosystems* 4 (art. no.-1030).
- Suhr, G., 1999. Melt migration under oceanic ridges: inferences from reactive transport modelling of upper mantle hosted dunites. *Journal of Petrology* 40, 575–599.
- Sun, S.-S., McDonough, W.F., 1989. Chemical and isotopic systematics of oceanic basalts: implications for mantle composition and processes. In: Saunders, A.D., Norry, M.J. (Eds.), *Magmatism in the Ocean Basins*. Geological Society Special Publication, pp. 313–345.
- Takazawa, E., Frey, F.A., Shimizu, N., Obata, M., Bodinier, J.L., 1992. Geochemical evidence for melt migration and reaction in the upper mantle. *Nature* 359, 55–58.
- Taylor, W.R., 1998. An experimental test of some geothermometer and geobarometer formulations for upper mantle peridotites with application to the thermobarometry of fertile lherzolite and garnet websterite. *Neues Jahrbuch Fur Mineralogie, Abhandlungen* 172, 381–408.
- Van Achtebergh, E., Ryan, C.G., Jackson, S.E., Griffin, W.L., 2001. Data reduction software for LA-ICP-MS. In: Sylvester, P.J. (Ed.), *Laser-Ablation-ICPMS in the Earth Sciences. Principles and Applications*. Mineralogical Association of Canada, pp. 239–243.

- Vasseur, G., Vernières, J., Bodinier, J.-L., 1991. Modelling of trace element transfer between Mantle melt and heterogranular peridotite matrix. *Journal of Petrology* 41–54.
- Vernières, J., Godard, M., Bodinier, J.L., 1997. A plate model for the simulation of trace element fractionation during partial melting and magma transport in the Earth's upper mantle. *Journal of Geophysical Research, Solid Earth* 102, 24771–24784.
- Vladimirov, V.G., Vladimirov, A.G., Gibsher, A.S., Travin, A.V., Rudnev, S.N., Shemelina, I.V., Barabash, N.V., Savinykh, Y.V., 2005. Model of the tectonometamorphic evolution for the Sangilen block (Southeastern Tuva, Central Asia) as a reflection of the early Caledonian accretion-collision tectogenesis. *Doklady Earth Sciences* 405, 1159–1165.
- Watson, E.B., Brenan, J.M., 1987. Fluids in the lithosphere. 1: Experimentally-determined wetting characteristics of CO<sub>2</sub>-H<sub>2</sub>O fluids and their implications for fluid transport, host-rock physical properties, and fluid inclusion formation. *Earth and Planetary Science Letters* 85, 497–515.
- Webb, S.A.C., Wood, B.J., 1986. Spinel-pyroxene-garnet relationships and their dependence on Cr/Al Ratio. *Contributions to Mineralogy and Petrology* 92, 471–480.
- Wiechert, U., Ionov, D.A., Wedepohl, K.H., 1997. Spinel peridotite xenoliths from the Atsagin-Dush volcano, Dariganga lava plateau, Mongolia: a record of partial melting and cryptic metasomatism in the upper mantle. *Contributions to Mineralogy and Petrology* 126, 345–364.
- Wilshire, H.G., 1987. A model of mantle metasomatism. *Geological Society of America Special Papers* 215, 47–60.
- Witt-Eickchen, G., Seck, H.A., 1991. Solubility of Ca and Al in Ortho-pyroxene from spinel peridotite — an improved version of an empirical geothermometer. *Contributions to Mineralogy and Petrology* 106, 431–439.
- Xu, Y.G., Menzies, M.A., Bodinier, J.L., Bedini, R.M., Vroon, P., Mercier, J.C.C., 1998. Melt percolation and reaction atop a plume: evidence from the poikiloblastic peridotite xenoliths from Borée (Massif Central, France). *Contributions to Mineralogy and Petrology* 132, 65–84.
- Xu, Y.G., Menzies, M.A., Thirlwall, M.F., Huang, X.L., Liu, Y., Chen, X.M., 2003. “Reactive” harzburgites from Huinan, NE China: Products of the lithosphere–asthenosphere interaction during lithospheric thinning? *Geochimica et Cosmochimica Acta* 67, 487–505.
- Yaxley, G.M., Cranford, A.J., Green, D.H., 1991. Evidence for carbonatite metasomatism in spinel peridotite xenoliths from western Victoria, Australia. *Earth and Planetary Science Letters* 107, 305–317.
- Zinngrebe, E., Foley, S.F., 1995. Metasomatism in mantle xenoliths from Gees, west Eifel, Germany—evidence for the genesis of calc-alkaline glasses and metasomatic Ca-enrichment. *Contributions to Mineralogy and Petrology* 122, 79–96.
- Zonenshain, L.P., Kuzmin, M.I., Natapov, L.M., Page, B.M., 1990. *Geology of the USSR: A Plate-Tectonic Synthesis*. AGU, Washington, D. C.
- Zorin, Y.A., Novoselova, M.R., Turutanov, E.K., Kozhevnikov, V.M., 1990. Structure of the lithosphere of the Mongolian–Siberian mountainous province. *Journal of Geodynamics* 11, 327–342.